PNAS

Supplementary Information for

Inhibition of RAS-driven signaling and tumorigenesis with a pan-RAS monobody targeting the Switch I/II pocket

Lauren Wallon[a,1], Imran Khan[b,c,1], Kai Wen Teng[a], Akiko Koide[a,d], Mariyam Zuberi[b,c], Jianping Li[e], Gayatri Ketavarapu[a], Nathaniel J. Traaseth[e], John P. O'Bryan[b,c,2], Shohei Koide[a,f,2]

[a]Laura and Isaac Perlmutter Cancer Center, New York University Langone Health, New York, NY 10016
[b]Department of Cell and Molecular Pharmacology and Experimental Therapeutics, Hollings Cancer Center, Medical University of South Carolina, Charleston, SC 29425
[c]Ralph H. Johnson VA Medical Center, Charleston, SC 29401
[d]Department of Medicine, New York University School of Medicine, New York, NY 10016
[e]Department of Chemistry, New York University, New York, NY, 10003
[f]Department of Biochemistry and Molecular Pharmacology, New York University School of Medicine, New York, NY 10016

[1]These authors contributed equally to this work.

[2]Correspondence to: Shohei Koide and John P. O'Bryan
Email: Shohei.Koide@nyulangone.org; obryanjo@musc.edu

This PDF file includes:

Figures S1 to S12
Tables S1 to S3
SI References

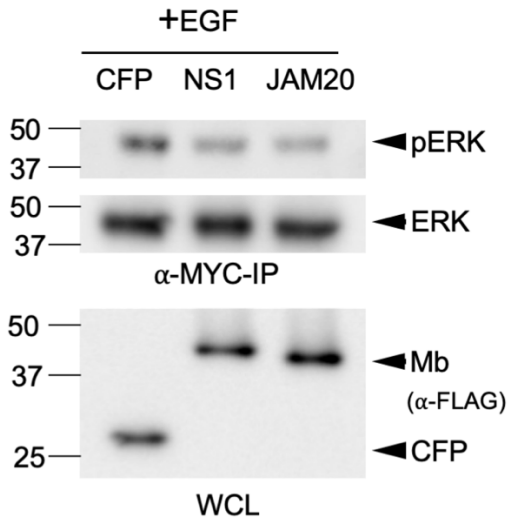

Fig. S1. Effect of CFP-JAM20 on EGF-stimulated ERK-MAPK activation in HEK293 cells. CFP-FLAG and CFP-NS1 were used as controls.

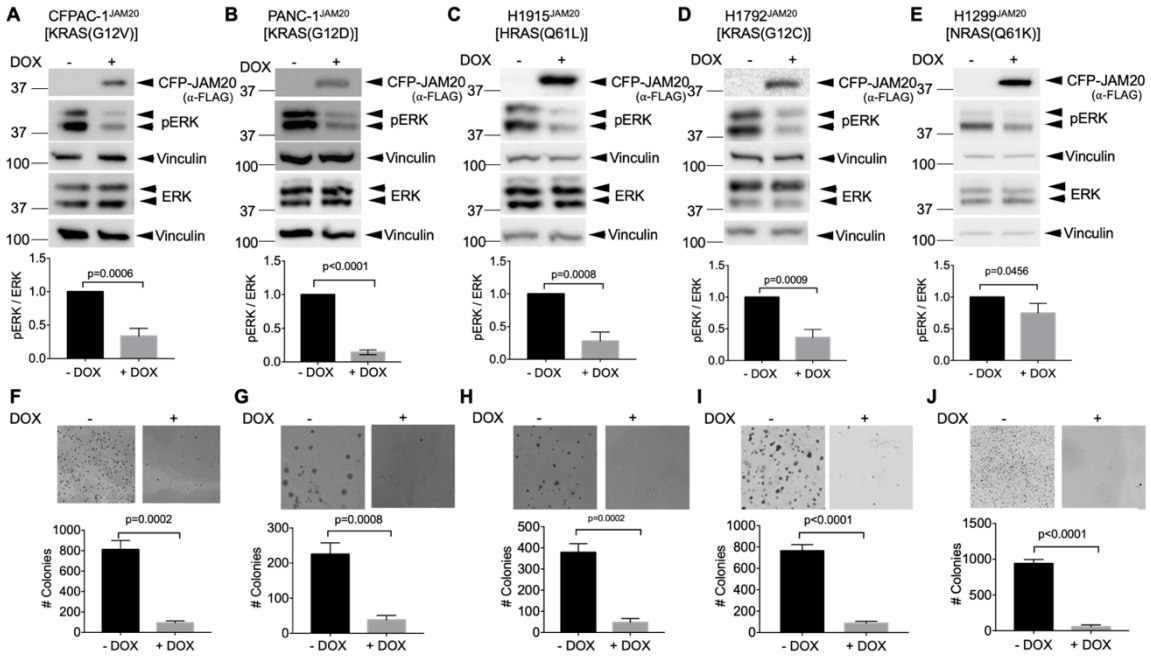

Fig. S2. DOX-regulated JAM20 expression inhibits signaling and growth of RAS mutant human tumor cell lines. a-e. Doxycycline (DOX) inducible JAM20 expressing stable lines were generated from *RAS* mutant tumor cells. ERK activation was then measured ±DOX treatment by Western blot analysis for pERK levels. The mutant RAS protein expressed in each tumor line is indicated above the panels. Vinculin expression was used as a control for loading. JAM20 expression reduced anchorage independent growth of RAS mutant human tumor cells. Engineered JAM20 cells were plated on soft agar in the absence (-) or presence (+) of DOX and allowed to grow for 3-4 weeks. f) CFPAC-1^{JAM20}, KRAS(G12V) mutant human pancreatic ductal adenocarcinoma tumor; g) PANC-1^{JAM20}, KRAS(G12D) mutant human pancreatic ductal adenocarcinoma tumor; h) H1915^{JAM20}, HRAS(Q61L) mutant human lung tumor; i) H1792^{JAM20}, KRAS(G12C) mutant human lung cancer cells; j) H1299^{JAM20}, NRAS(Q61K) lung cancer cells. Graphs represent the average colony number from three wells ± s.d. Colonies were counted using NIH ImageJ software. Images are representative wells from each assay. *P* values were determined by comparison of colony numbers between – and +DOX conditions using a student's t-test.

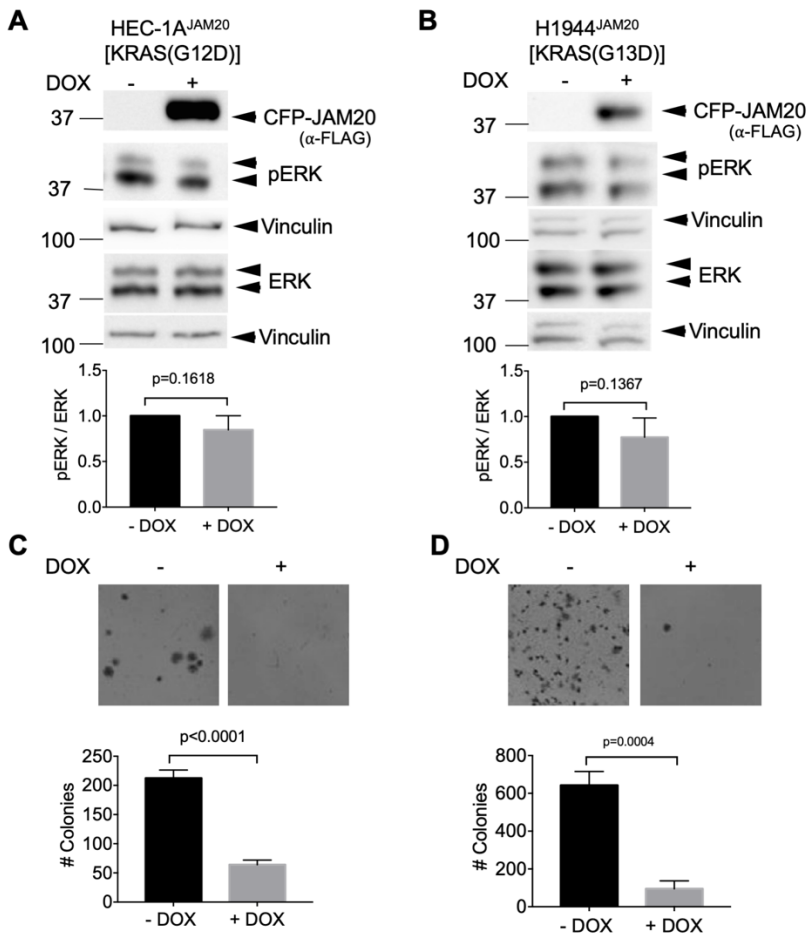

Fig. S3. Evaluating DOX-regulated JAM20 expression on signaling and growth of RAS mutant human tumor cell lines. (A-B) Doxycycline (DOX) inducible JAM20 expressing stable lines were generated from *RAS* mutant tumor cells. ERK activation was then measured ±DOX treatment by Western blot analysis for pERK levels. The mutant RAS protein expressed in each tumor line is indicated above the panels. Vinculin expression was used as a control for loading. (C-D) JAM20 expression reduced anchorage independent growth of RAS mutant human tumor cells. Engineered JAM20 cells were plated on soft agar in the absence (-) or presence (+) of DOX and allowed to grow for 3-4 weeks. (C) HEC-1A^{JAM20}, KRAS(G12D) mutant human endometrial adenocarcinoma tumor; (D) H1944^{JAM20}, KRAS(G13D) mutant human non-small cell lung carcinoma tumor. Graphs represent the average colony number from three wells ± s.d. Colonies were counted using NIH ImageJ software. Images are representative wells from each assay. *P* values were determined by comparison of colony numbers between – and +DOX conditions using a student's t-test.

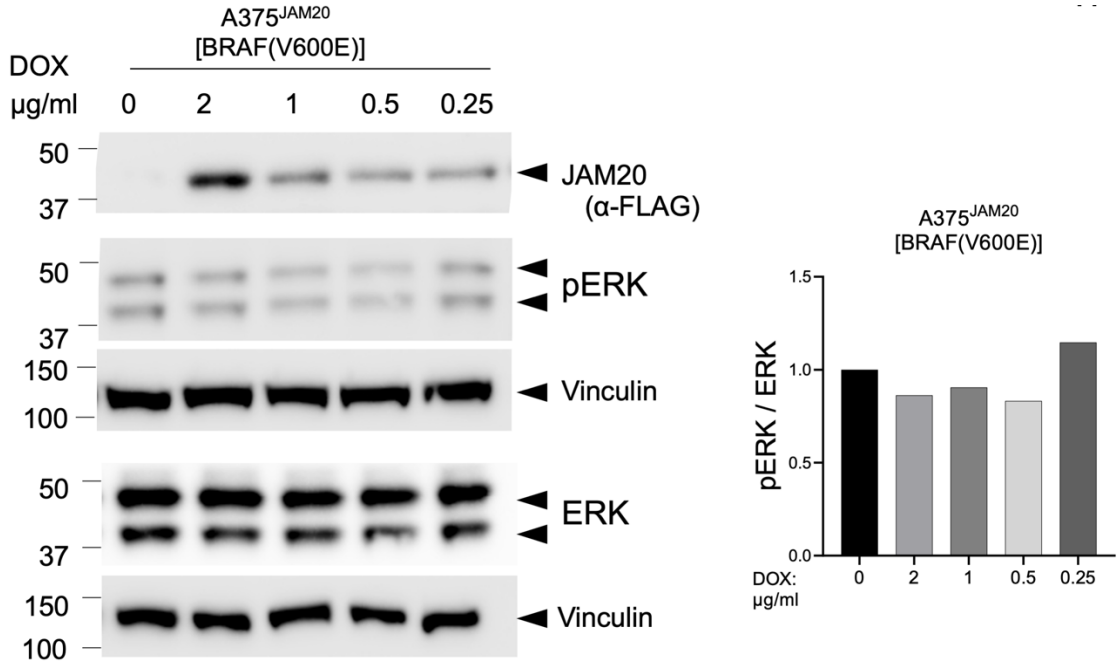

Fig. S4. Titration of DOX induced JAM20 expression on ERK-MAPK signaling in BRAF(V600E) mutant A375 melanoma cells. Experiments were performed as described in Fig. S2 A-E.

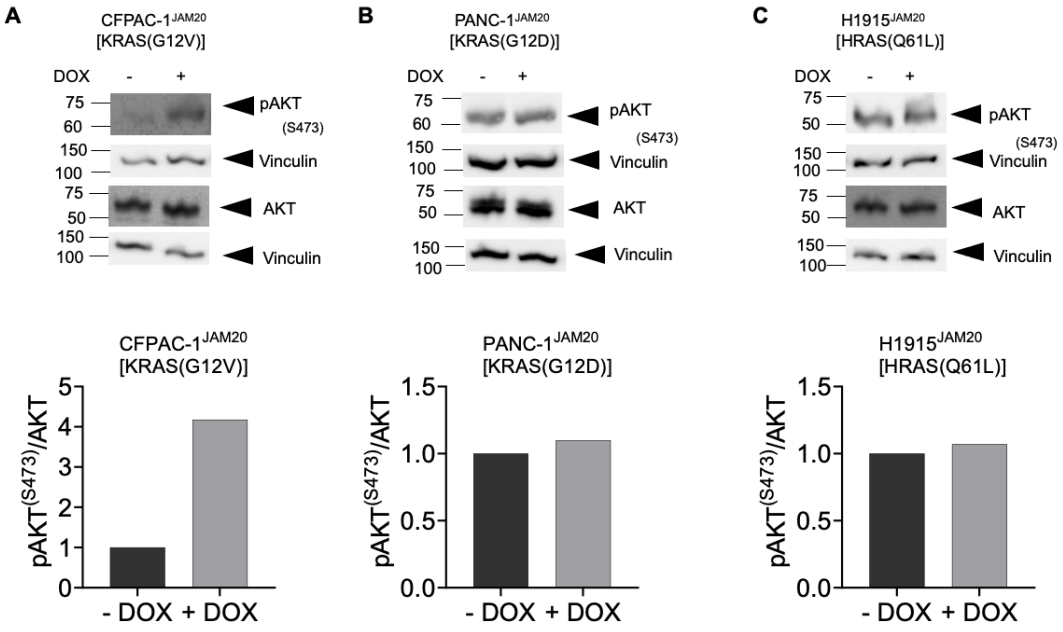

Fig. S5. Effect of JAM20 expression on AKT activation in 2D growth conditions. Experiments were performed as in Fig. S2 A-E, but blots were probed for AKT activation using phospho-specific AKT antibodies (pAKT^{S473}).

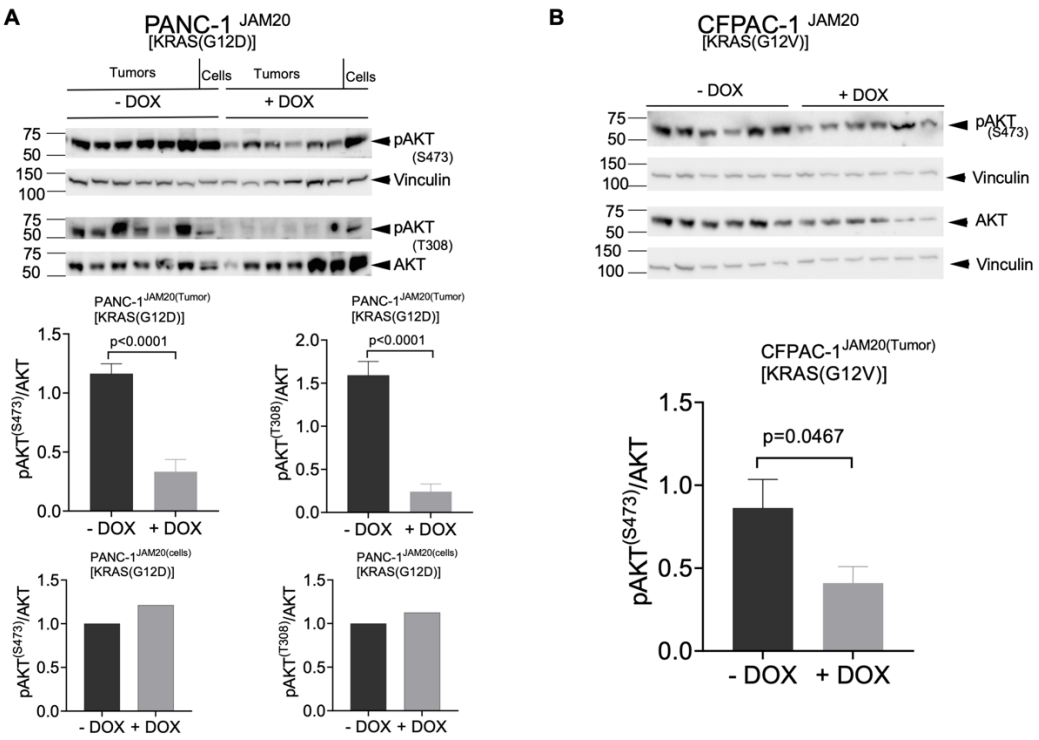

Fig. S6. Effect of JAM20 expression on AKT activation in tumor lysates as shown in Fig. 3a-b. Athymic nude mice were injected subcutaneously in the flanks with either (A) PANC-1^{JAM20} or (B) CFPAC-1^{JAM20} cells. Mice were divided into two cohorts treated without (-) or with (+) DOX and monitored for tumor development.

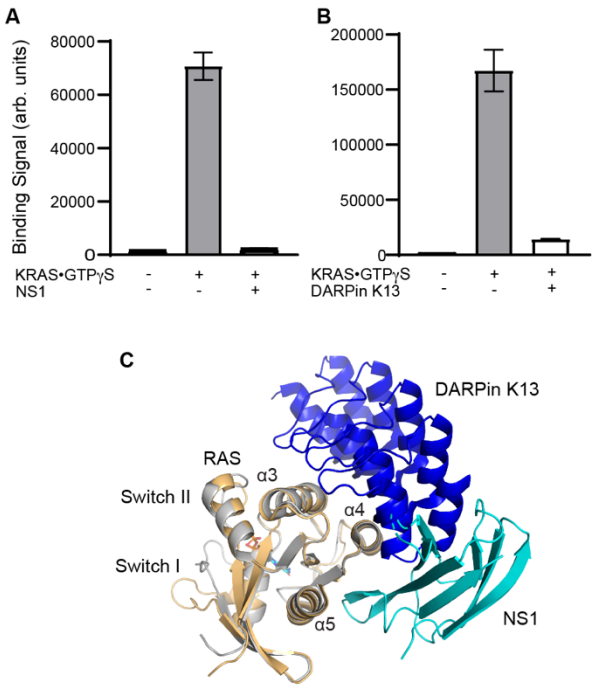

Fig. S7. Competitive binding of NS1 and DARPin K13. Binding of 100nM biotinylated KRAS(WT)•GTPγS to NS1 displayed on the yeast surface in the presence and absence of 1 μM purified NS1 (a) or DARPin K13 (b) was measured using flow cytometry. The mean and s.d. of three technical replicates are plotted. c) Overlay of the DARPin K13-KRAS(WT)•GDP complex (PDB ID 6H46) and NS1-HRAS(WT)•GDP complex (PDB ID 5E95) using the RAS structures as the reference.

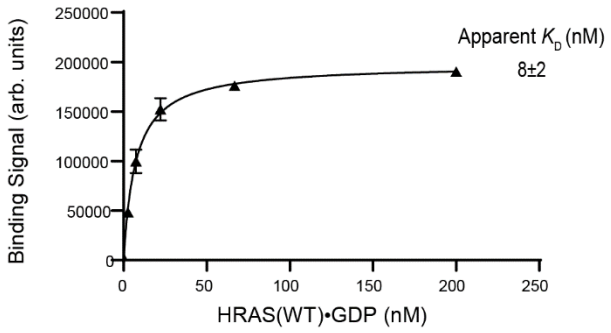

Fig. S8. Binding titration measurements of JAM20(Y83S) against HRAS(WT)•GDP using yeast display. The mean and s.d. of three technical replicates are plotted.

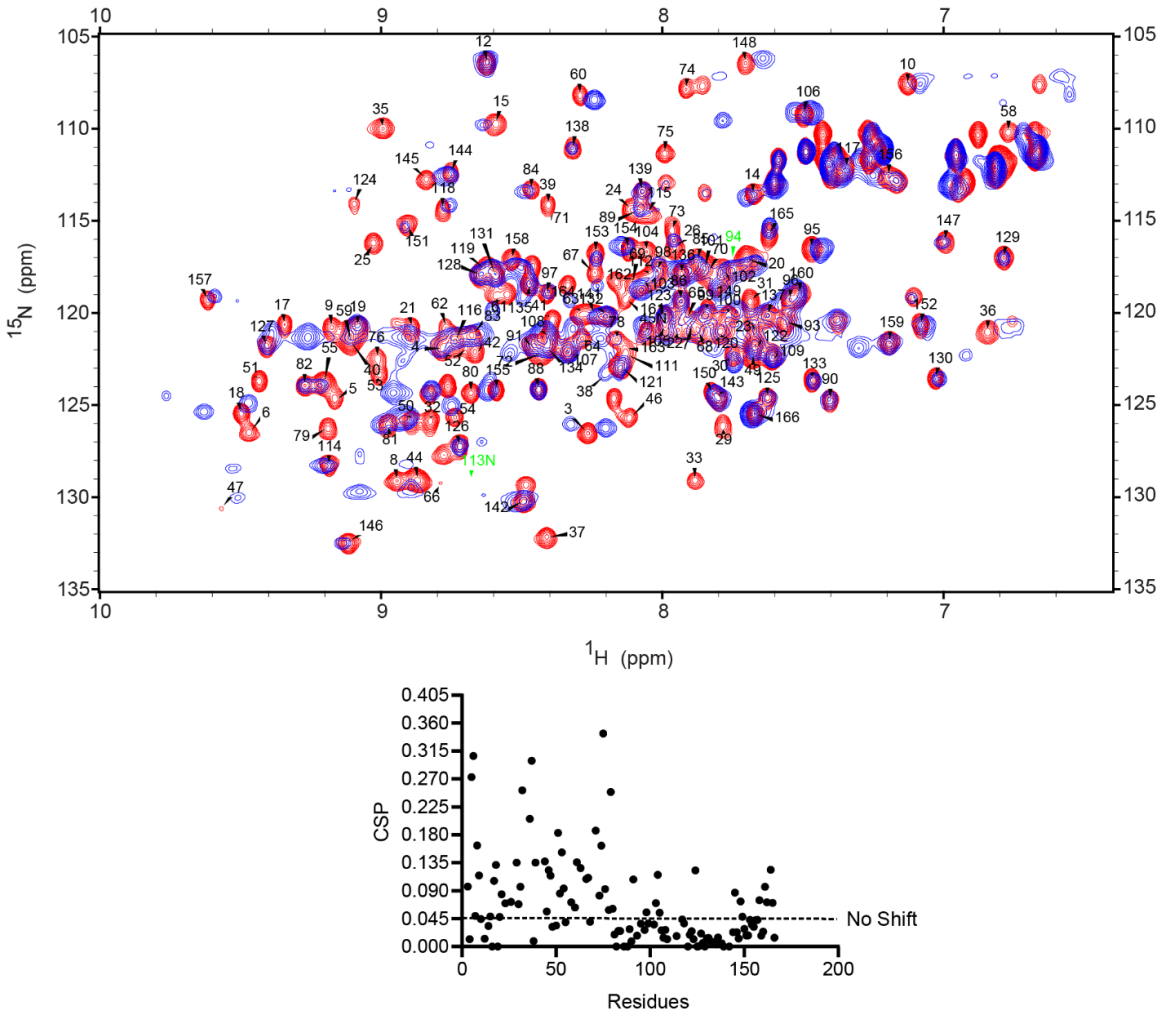

Fig. S9. Spectra for HSCQ-NMR. HRAS(WT)- Only spectra is shown in red and HRAS(WT) complexed with JAM20(Y83S) is shown in purple. Chemical shift perturbation (CSP) plot shows assigned residues where the cut-off for movement was placed at 0.045. The following residues were not unambiguously assigned in the spectra and consequently not included in this plot: 11, 22, 24, 25, 29, 35, 40, 41, 42, 49, 59, 62, 64, 65, 69, 70, 72, 85, 94, 92, 96, 100, 101, 111, 112, 113, 115, 116, 119, 134, 141, 143, 163.

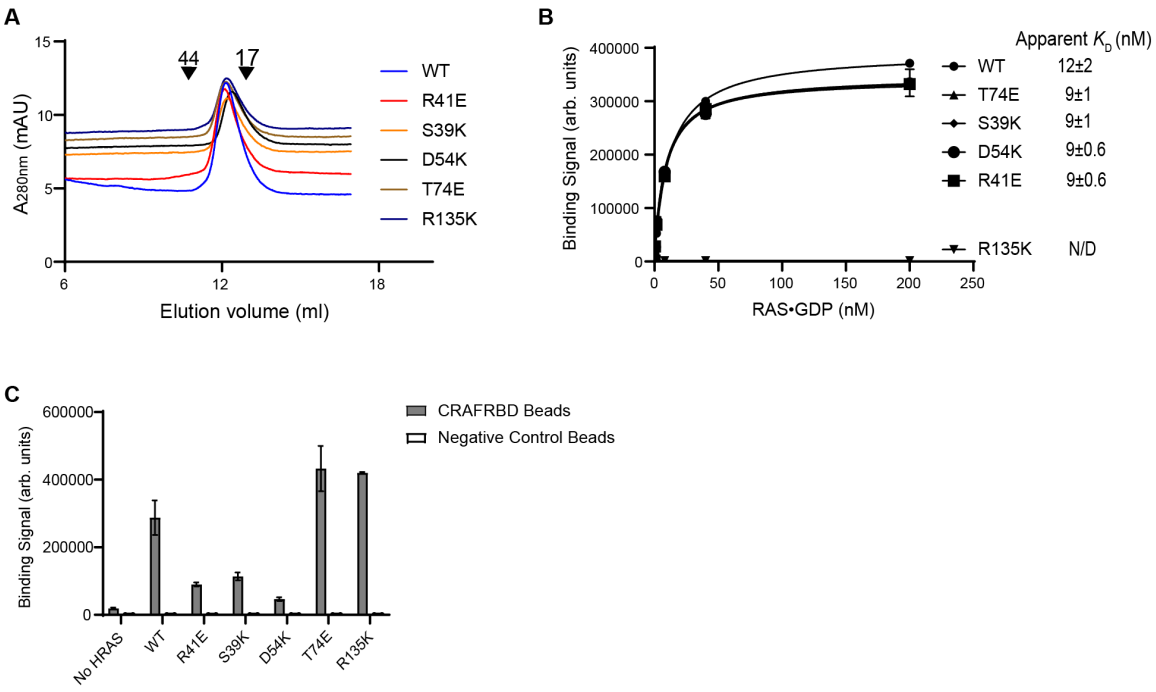

Fig. S10. Assessing HRAS variants. (A) Size-exclusion chromatography analysis. Five μM of HRAS-WT or 2.9 μM of HRAS variant (R41E, S39K, D54K, T74E or R135K) were injected into a Superdex S75 10/300 column and the absorbance at 280 nm was detected. The arrows with 44 and 17 represent the elution positions of molecular weight standards. n=1. (B) Evaluating the structural integrity of HRAS variants via NS1 binding. Binding of purified HRAS mutants to NS1 on the yeast surface was measured using flow cytometry. The mean and s.d. of three technical replicates are plotted. ND, Not Determined. (C) Binding of RAF(RBD) binding to HRAS variants. Binding of purified HRAS•GTPγS variants (250 nM) to biotinylated RAF(RBD) immobilized on streptavidin M280 beads was measured using flow cytometry. The mean and s.d. of three technical replicates are plotted.

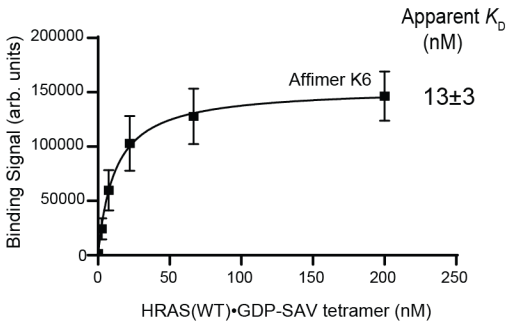

Fig. S11. Binding titration of HRAS(WT)•GDP precomplexed with streptavidin to affimer K6 displayed on yeast surface. The use of the HRAS-streptavidin complex results in substantial affinity enhancement due to multivalent interactions, which enables the detection of weak interactions. The HRAS concentration is expressed in terms of the HRAS monomer.

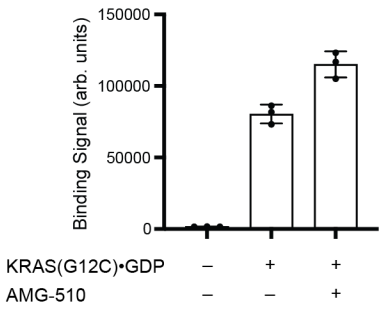

Fig. S12. Effect of AMG-510 conjugation to KRAS(G12C)•GTP on the binding of JAM20 as tested in the yeast display format. JAM20 was displayed on the yeast surface. KRAS(G12C)•GDP was treated with AMG-510 prior to the binding measurements. The final concentration of KRAS(G12C) was 8 nM. The graph shows the mean and s.d. of technical triplicates, representative of n=2 independent experiments.

Table S1. Amino acid sequences of monobodies used in this study

Construct	Amino acid sequence
JAM20	VSSVPTKLEVVAATPTSLLISWDASSSSVSYYRITYGETGGNSPVQEFTVPSYYSTAT ISGLKPGVDYTITVYAYYWYGSPYYYWKASPISINYRT
Mb(Neg)	VSSVPTKLEVVAATPTSLLISWDASSSSVSYYRITYGETGGNSPVQEFTVPGSKSTAT ISGLKPGVDYTITVYASSSSSSSSSSSKPISINYRT
pHBT-JAM20	MKHHHHHHSSGLNDIFEAQKIEWHEENLYFQGSVSSVPTKLEVVAATPTSLLISWDAS SSSVSYYRITYGETGGNSPVQEFTVPSYYSTATISGLKPGVDYTITVYAYYWYGSPYY YWKASPISINYRT (N-terminal tag is underlined; TEV cleavage occurs C-terminal to the ENLYFQ sequence)
ECFP-FLAG-JAM20	MVSKGEELFTGVVPILVELDGDVNGHKFSVSGEGEGDATYGKLTLKFICTTGKLPVPW PTLVTTLTWGVQCFSRYPDHMKQHDFFKSAMPEGYVQERTIFFKDDGNYKTRAEVKFE GDTLVNRIELKGIDFKEDGNILGHKLEYNYISHNVYITADKQKNGIKANFKIRHNIED GSVQLADHYQQNTPIGDGPVLLPDNHYLSTQSALSKDPNEKRDHMVLLEFVTAAGITL GMDELYKSGLRSRDYKDDDDKGSGSVSSVPTKLEVVAATPTSLLISWDASSSSVSYYR ITYGETGGNSPVQEFTVPSYYSTATISGLKPGVDYTITVYAYYWYGSPYYYWKASPIS INYRT (N-terminal tag, ECFP-FLAG, is underlined)

Table S2. Description of cell lines used, their origin and the mutational status

Cell Line	Origin	RAS Mutation
CFPAC-1	Pancreatic ductal adenocarcinoma	KRAS(G12V)
PANC-1	Pancreatic ductal adenocarcinoma	KRAS(G12D)
NCI-H1915	Non-small cell lung carcinoma	HRAS(Q61L)
NCI-H1944	Non-small cell lung carcinoma	KRAS(G13D)
NCI-H1299	Non-small cell lung carcinoma	NRAS(Q61K)
HEC-1A	Endometrial adenocarcinoma	KRAS(G12D)
NCI-H1792	Lung Adenocarcinoma	KRAS(G12C)
A375	Melanoma	BRAF(V600E)

Table S3. Summary of RAS-targeting biologics that can be used as genetically encoded reagents

Name	Platform	Isotype specificity	Mutation specificity	Nucleotide specificity	affinity (lowest K_D or IC_{50}, nM)	Epitope	PDB ID	Ref
iDab#6	VH	none	none	GTP	6	SI, SII	2VH5	1
K55	DARPin	none	none	GTP	167	SI, SII	5MLA	2
RBDv1	RBD	RAS, RAP	none	GTP	3	SI	6NTC	3
RBDv12	RBD	RAS, RAP	none	GTP	3	SI	6NTD	3
12VC1	Monobody	ND	G12C, G12V	GTP	25	SI, SII, P-loop	7L0G	4
K27	DARPin	none	none	GDP	3.9	SI, SII	5O2T	2
R11.1.6	Sso7d	ND	preference for G12D in the GTP state	GDP	3	SI/SII pocket	5UFE	5
K6	Affimer	ND	ND	none	592*	SI/SII pocket	6YR8	6
JAM20	Monobody	none	none	GDP	5	SI/SII pocket		This work
K3	Affimer	KRAS	ND	none	144*	SII pocket	6YXW	6
R15	Monobody	none	fast cycling mutants (in cells)	nucleotide free	28	ND		7
NS1	Monobody	HRAS, KRAS	none	none	14	α4-β6-α5	5E95	8
K69	Affimer	ND	ND	none	697*	α4-β6-α5	7NY8	6
K13	DARPin	KRAS	none	none	127*	α3-α4	6H46	9
K19	DARPin	KRAS	none	none	7*	α3-α4	6H47	9

Molecules exhibiting different types of specificity are separated with thick lines. ND, not determined. *IC_{50} values.

SI References

1. Tanaka T, Williams RL, & Rabbitts TH (2007) Tumour prevention by a single antibody domain targeting the interaction of signal transduction proteins with RAS. *EMBO J* 26:3250-3259.
2. Guillard S*, et al.* (2017) Structural and functional characterization of a DARPin which inhibits Ras nucleotide exchange. *Nat Commun* 8:16111.
3. Wiechmann S*, et al.* (2020) Conformation-specific inhibitors of activated Ras GTPases reveal limited Ras dependency of patient-derived cancer organoids. *J Biol Chem* 295:4526-4540.
4. Teng KW*, et al.* (2021) Selective and noncovalent targeting of RAS mutants for inhibition and degradation. *Nat Commun* 12:2656.
5. Kauke MJ*, et al.* (2017) An engineered protein antagonist of K-Ras/B-Raf interaction. *Sci Rep* 7:5831.
6. Haza KZ*, et al.* (2021) RAS-inhibiting biologics identify and probe druggable pockets including an SII-alpha3 allosteric site. *Nat Commun* 12:4045.
7. Khan I*, et al.* (2022) Identification of the nucleotide-free state as a therapeutic vulnerability for inhibition of selected oncogenic RAS mutants. *Cell Rep* 38:110322.
8. Spencer-Smith R*, et al.* (2017) Inhibition of RAS function through targeting an allosteric regulatory site. *Nat Chem Biol* 13:62-68.
9. Bery N*, et al.* (2019) KRAS-specific inhibition using a DARPin binding to a site in the allosteric lobe. *Nat Commun* 10:2607.